University of Anbar
college of science
physics department

health physics

by. Dr.Essmat Ramizy Al-hadithi

X- RAY

References

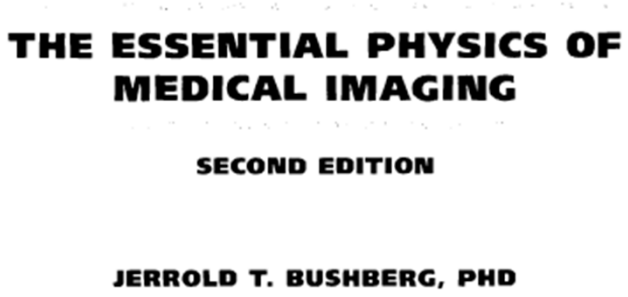

Health
Physics
FO UR TH EDITIO N
Herman Cember, PhD
Professor Emeritus
Northwestern University
Evanston, Illinois

Gamma Emitters

For gamma-emitting isotopes, we cannot simply calculate the absorbed dose by assuming the organ to be infinitely large because gammas, being penetrating radiations, may travel great distances within the tissue and leave the tissue without interacting. Thus, only a fraction of the energy carried by photons originating in the radioisotope-containing tissue is absorbed within that tissue. Before the advent of computers that made complex computational methods possible, gamma ray doses from internal radio nuclides were calculated by assuming the body to be made of spheres and cylinders and then using simple calculation techniques to determine internal dose. For example, in the case of a uniformly distributed gamma-emitting nuclide, the dose rate at any point p due to the radioactivity in the volume dV at any other point at a distance r from point p, as shown in Figure

$$dD = C\Gamma\frac{e^{-\mu r}}{r^2}dV,$$

where C is the concentration of the isotope, is the specific gamma-ray emission, and μ is the linear energy absorption coefficient. The dose rate at point p due to all

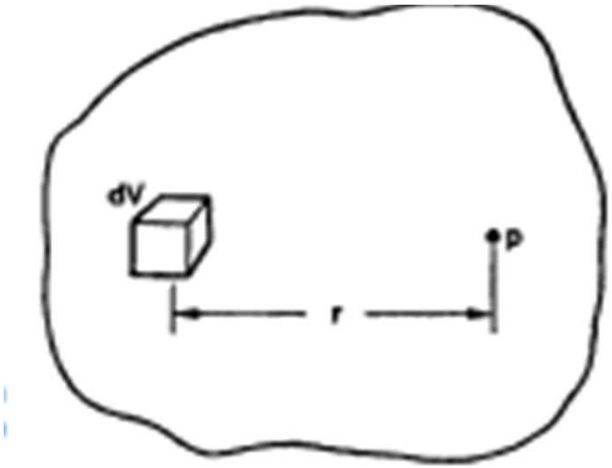

the isotope in the tissue is computed by the contributions from all the infinitesimal volume elements:

$$\dot{D} = CT \int_0^V \frac{e^{-\mu r}}{r^2} dV. \tag{6.64}$$

For the case of a sphere, the dose rate at the center (Fig. 6-9) is

$$\dot{D} = 4CT \int_{r=0}^{r=R} \int_{\theta=0}^{\theta=\pi/2} \int_{\varphi=0}^{\varphi=\pi} \frac{e^{-\mu r}}{r^2} \cdot r\,d\theta \cdot r\cos\theta\,d\varphi \cdot dr. \tag{6.65}$$

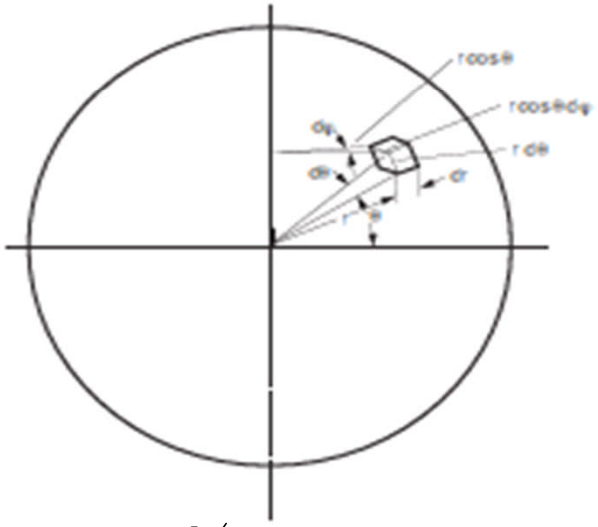

$$D_\beta = 21.24\times10^5 CT \; rad/hr$$

TABLE 6-4. *Average Geometry Factors for Cylinders Containing a Uniformly Distributed Gamma Emitter*

CYLINDER HEIGHT (cm)	RADIUS OF CYLINDER (cm)							
	3	5	10	15	20	25	30	35
2	17.5	22.1	30.3	34.0	36.2	37.5	38.6	39.3
5	22.3	31.8	47.7	56.4	61.6	65.2	67.9	70.5
10	25.1	38.1	61.3	76.1	86.5	93.4	98.4	103
20	25.7	40.5	68.9	89.8	106	117	126	133
30	25.9	41.0	71.3	94.6	112	126	137	146
40	25.9	41.3	72.4	96.5	116	131	143	153
60	26.0	41.6	73.0	97.8	118	134	148	159
80	26.0	41.6	73.3	98.4	119	135	150	161
100	26.0	41.6	73.3	98.5	119	136	150	162

Integrating with respect to each of the variables, we have, for the dose rate at the center of the sphere,

$$\dot{D} = CT \cdot \frac{4\pi}{\mu}\left(1 - e^{-\mu R}\right). \tag{6.66}$$

From an examination of Eqs. (6.63), (6.64), (6.65), and (6.66) it is seen that the factor that multiplies CT depends only on the geometry of the tissue mass and hence is called the *geometry factor*.[1] The geometry factor g is defined by

$$g = \int_0^V \frac{e^{-\mu r}}{r^2} dV. \tag{6.67}$$

Equation (6.64) may therefore be rewritten as

$$D = C \times \Gamma \times g. \tag{6.68}$$

The definition of g in Eq. (6.67) applies to a given point within a volume of tissue. In many health physics instances, we are interested in the average dose rate rather than the dose rate at a specific point. For this purpose, we may define an average geometry factor as follows:

$$\bar{g} = \frac{1}{V}\int g\,dV. \tag{6.69}$$

For a sphere,

$$\bar{g} = \frac{3}{4}(g)_{center}. \tag{6.70}$$

At any other point in the sphere at a distance d from the center, the geometry factor is given by

$$g_p = (g)_{center}\left[0.5 + \frac{1-(d/R)^2}{4(d/R)}\ln\frac{1+d/R}{|1-d/R|}\right]. \tag{6.71}$$

X-ray Production

When a beam of monoenergetic electrons that had been accelerated across a high potential difference is abruptly decelerated by stopping the electron beam (as in the case of an X-ray tube, a cathode ray tube, or a klystron microwave generator), a small fraction of the energy in the electron beam is converted into X-rays.

$$f_e = 1 \times 10^{-3} \times ZE,$$

where

f_e = fraction of the energy in the electron beam that is converted into X-rays,
Z = atomic number of the target in the X-ray tube or whatever the electron beam strikes in any other device, and
E = voltage across the X-ray tube or other device (mega volts, MV). The numerical value of the voltage E is equal to the kinetic energy of the electron, expressed in eV, as it strikes the target. Thus, an electron that has been accelerated across a voltage of 0.1 MV has acquired a kinetic energy of 0.1 MeV (or 100 keV).

This is the operating principle of traditional diagnostic, industrial, and analytical X-ray tube (Fig. 5-8). The American physicist William D. Coolidge invented this type of X-ray tube in 1913. In 1937, Dr. Coolidge was awarded an honorary MD degree by the University of Zurich in recognition of his many contributions of physics to medical science. It is interesting to note that Coolidge lived to the age of 101 years, despite his extensive experience with X-rays.

An electron beam, usually on the order of milliamperes, is generated by heating the cathode. A voltage difference on the order of tens to hundreds of kilo volts across the tube accelerates the electrons to form a monoenergetic beam in which the kinetic energy of the electrons in electron volts is numerically equal to the voltage across the tube. The high-speed electrons are stopped by a high-atomic-numbered metal target

that is embedded in the anode. Some of the kinetic energy in the electron beam is converted into X-rays (bremsstrahlung) when the electrons are suddenly stopped. In X-ray generators where the voltage is less than several hundred thousand volts, the X-rays (photons) are emitted mainly at angles around 90° to the direction of the electron beam. A hole in the protective shielding that houses the X-ray tube allows a useful X-ray beam to emerge from the shielded tube.

The X-rays that are produced in this manner have a continuous energy distribution that approaches a maximum energy equal to the kinetic energy of the electron that was stopped instantaneously and thus all of its kinetic energy was converted into an X-ray photon. If an electron were to be instantaneously stopped by the target, all of its kinetic energy would be converted into an X-ray photon. This would represent the maximum-energy (or shortest-wavelength) photon possible with the given voltage across the tube. However, this maximum limit can only be approached, since no electron can be stopped instantaneously. The fact that the electrons are slowed down at different rates due to different ionization and excitation collisions leads to a continuous energy distribution up to the theoretical maximum energy that is determined only by the high voltage across the X-ray tube (Fig. 5-9). If we have a full-wave rectified, but unfiltered AC voltage across the X-ray tube, then the voltage

The power, P watts, in the electron beam of an X-ray machine is given by the product of the high voltage across the tube, V volts, and the beam current i amperes.

$$P\,(\text{beam}) = V \times i.$$

Since the fraction of the beam power that is converted to X-rays is proportional to ZV, the intensity of the X-ray beam, I, is proportional to the product of ZV and Vi:

$$I(\text{X-rays}) \propto (ZV \times Vi) \propto ZV^2 i.$$

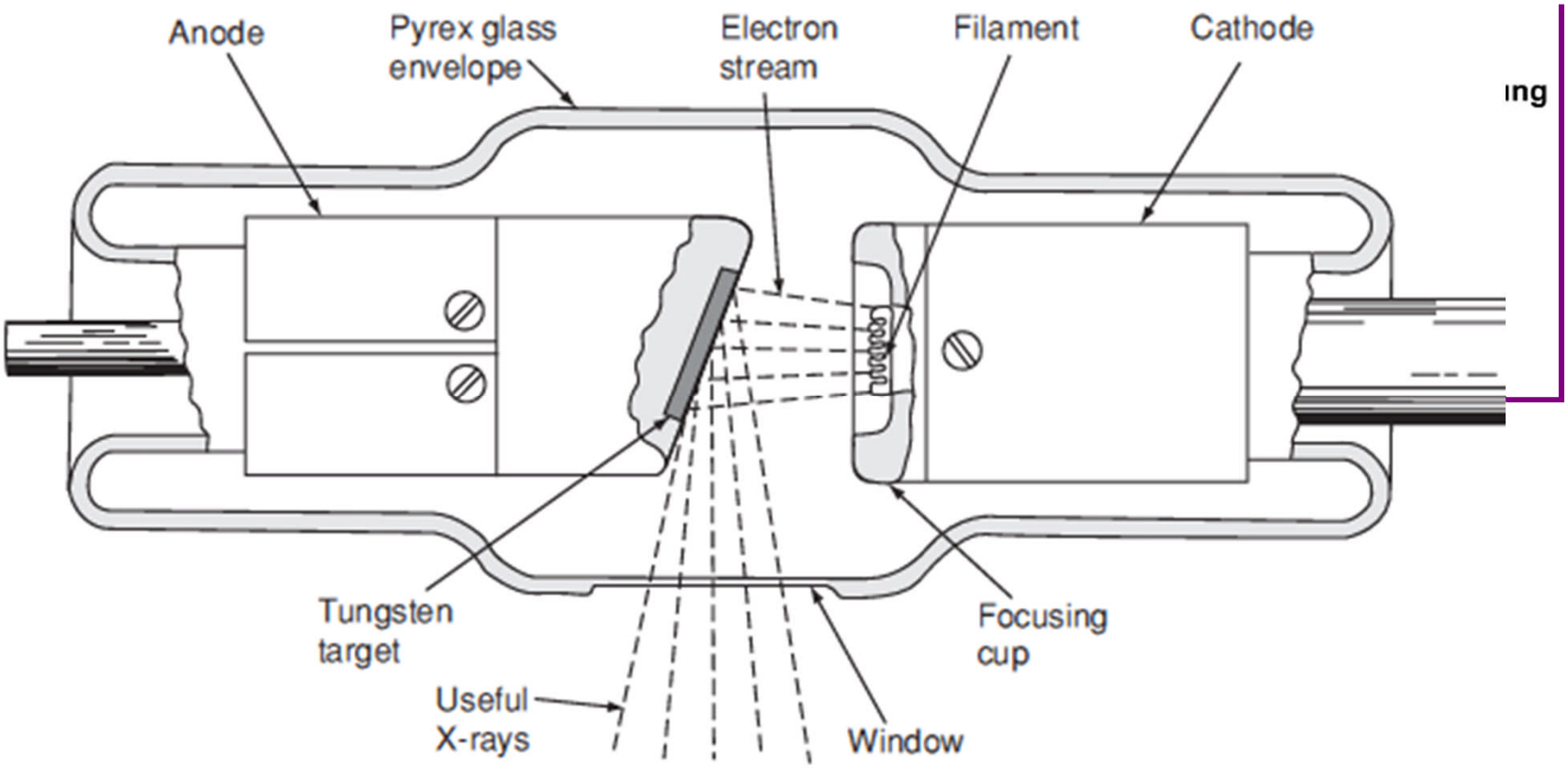

Typical operation conditions are:

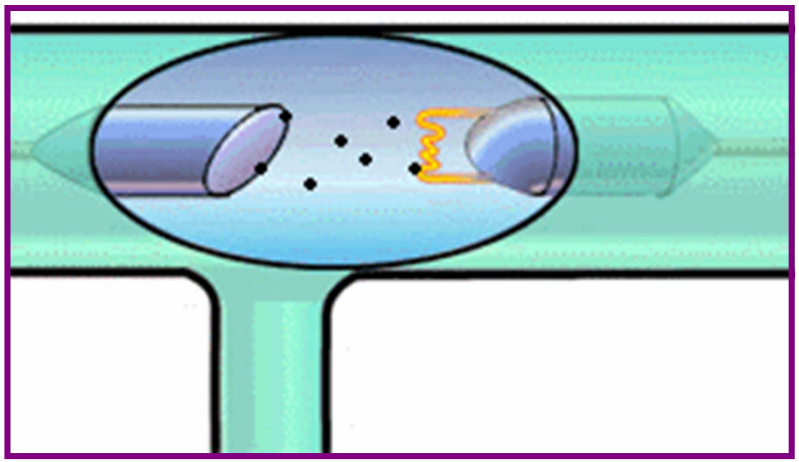

Acceleration Voltage: 20 to 150 kV

Electron Current: 1 to 5 mA (for continuous operation)

Electron Current: 0.1 to 1.0 A (for short exposures)

The radiographic image of the X-ray exposure is determined by the interaction of the X-rays which are transmitted through the patient with a photon detector (film, camera etc.)

Primary X-ray photons have passed through the patient without interaction, they carry useful information.
They give a measure for the probability that a photon pass through the patient without interaction which is a function of the body tissue attenuation coefficients.

Secondary photons result from interaction inside the patient, they are usually deflected from their original direction and carry therefore only little information. They create background noise which degrades the contrast of the image.

Scattered photons are often absorbed in grids between the patient and the image receptor.

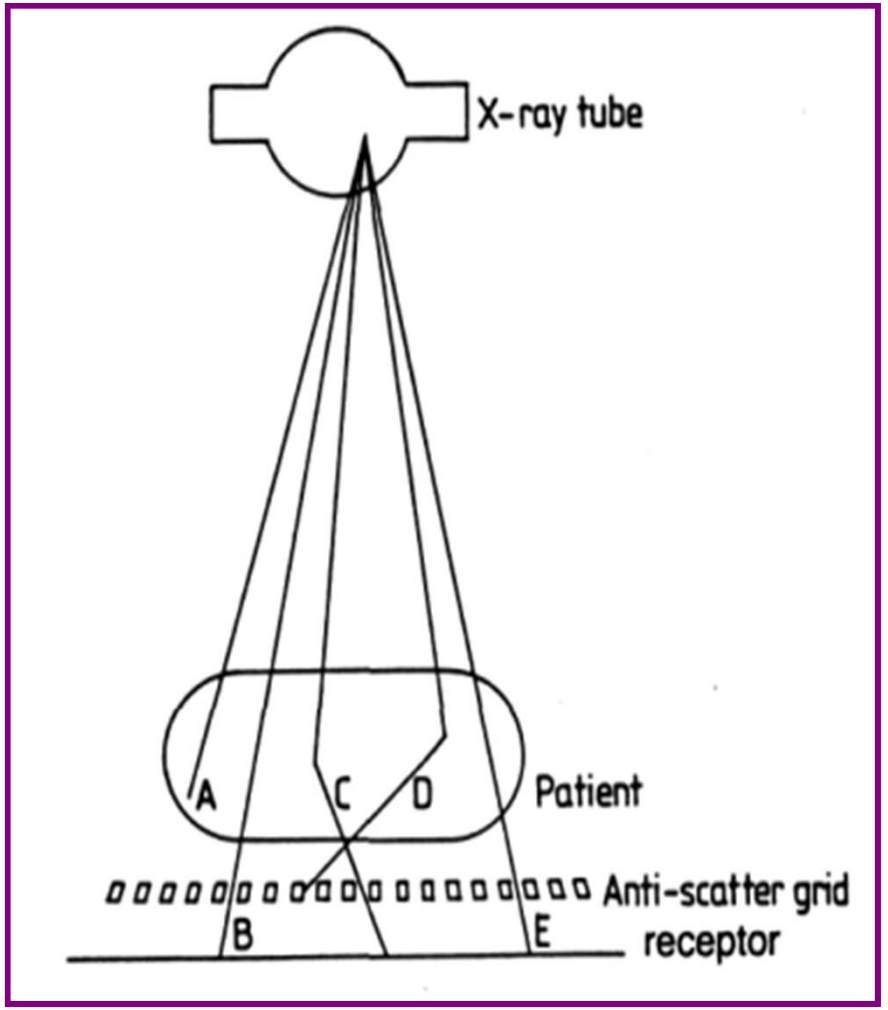

The two dimensional image *I*(*x, y*) of the three dimensional distribution of the X-ray attenuating body tissue of the patient can be described as a function of the initial photon intensity *N* of energy *E*, the energy absorption efficiency of the image receptor *ε*(*E*) (film) and the attenuation coefficients *μ* which have to be considered along the photon path in z-direction.

$$I(x,y) = \int (N(E) \cdot \epsilon(E) \cdot E \cdot e^{(-\int \mu(x,y,z)dz)} + S(E) \cdot \epsilon(E) \cdot E)dE$$

with *S*(*E*) as distribution of the scattered secondary X-ray photons.

The expression can be simplified to:

$$I(x,y) = \int N(E) \cdot \epsilon(E) \cdot E \cdot e^{(-\int \mu(x,y,z)dz)}(1+R)dE$$

with *R* as the ratio of secondary to primary radiation.

The **contrast** C **of the target tissue volume is defined in terms of the image distribution function** I_1 **and** I_2**:**

$$C = \frac{I_1 - I_2}{I_1}$$

I_1 **gives the energy absorbed outside the target tissue**

I_2 **gives the energy absorbed inside the target volume.**

Approximating for an X-ray energy E:

$$I_1 = N \cdot \epsilon(E) \cdot E \cdot e^{(-\mu_1 t)} + S \cdot \epsilon(E)E$$

$$I_2 = N \cdot \epsilon(E) \cdot E \cdot e^{(-\mu_1 (t-x) - \mu_2 x)} + S \cdot \epsilon(E)E$$

This yields for the contrast C:

$$C = N \cdot \epsilon(E) \cdot E \cdot e^{-\mu_1 t} \cdot (1 - e^{[-(\mu_2 - \mu_1)x]})/I_1$$

$$C = \frac{(1 - e^{(\mu_1 - \mu_2)x})}{(1 + R)}$$

The contrast depends mainly on the difference of attenuation coefficients μ_1 **and** μ_2 **as well as on the ratio of scattered to primary X-ray photons.**


kV
mAs


kV
%.mAs
150 200 300 400 500

TEST	K.V	mAs	TEST	K.V	mAs
Skull	56	20	Hand	41	1.8
Baby skull	48	12,16	ankle	46	6
Jaw	46	8	thigh	55	12
Baby chest	44	5	shoulder	48	4.5
Chest	50	12	Nike	66	32
Wrist	44	4	Chest(on desk)	58	10
Elbow	45	4	Arms	48	6.3
Baby wrist	40	2			
Baby Pelvis	44	3.2			
The leg	45	6			
knee	46	6			
Baby knee	42	2			
foot	43	3.2			
Baby foot	40	1			
Baby abdomen	45	6			
nose	41	3			
Splinted Leg	48	16			

Goose neck sign: Endocardial cushion defects

Scimitar sign: Partial anomalous pulmonary venous return

Figure of 8/ Snowman appearance: Total anomalous pulmonary venous connection (TAPVC)

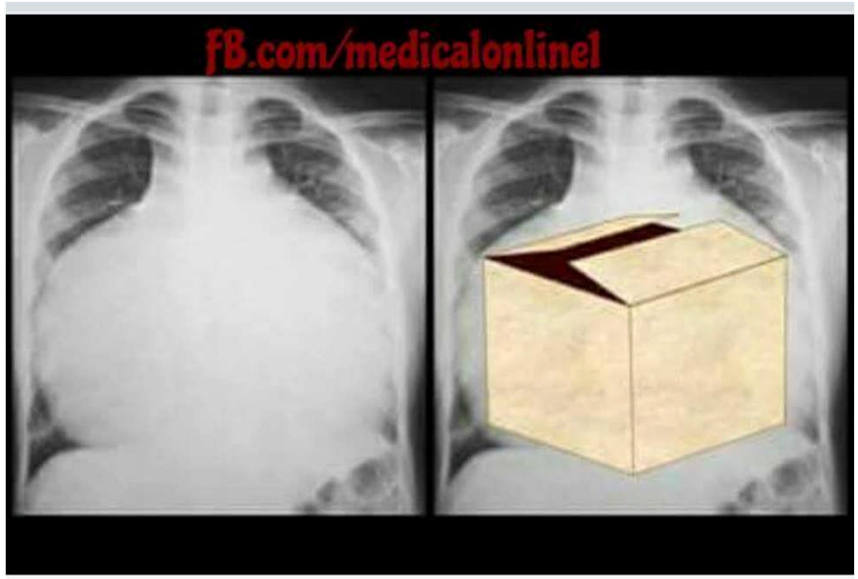

Box shaped heart: Ebstein's anomaly

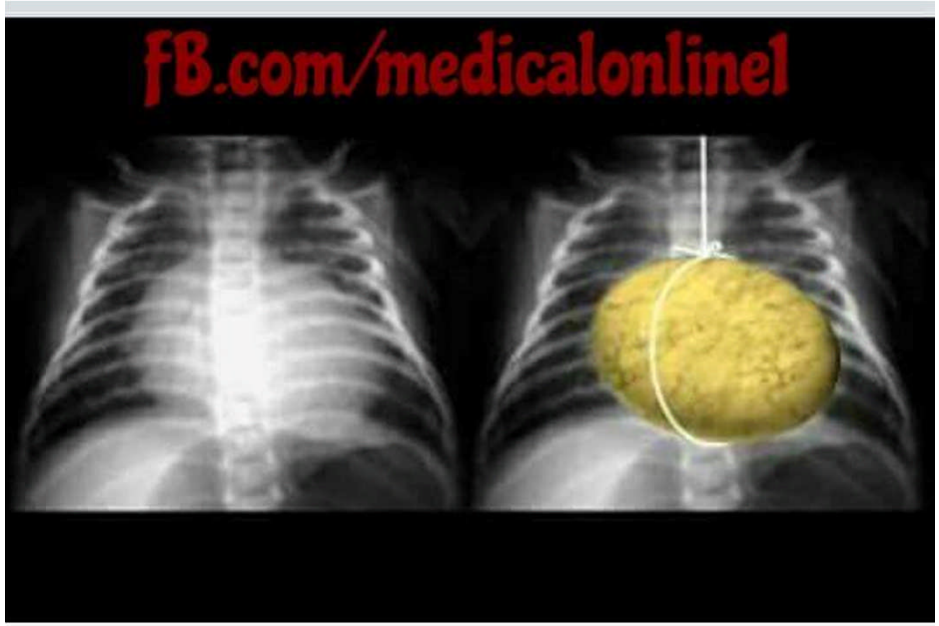

Egg on string/ Egg on side appearance: Transposition of great arteries (TGA)

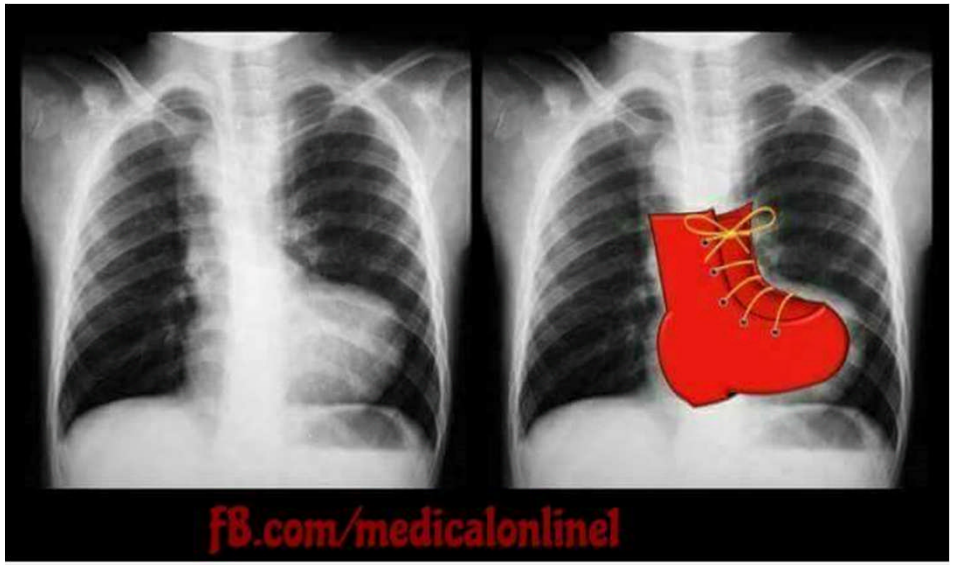

Boot shaped heart: Tetralogy of Fallot (TOF)

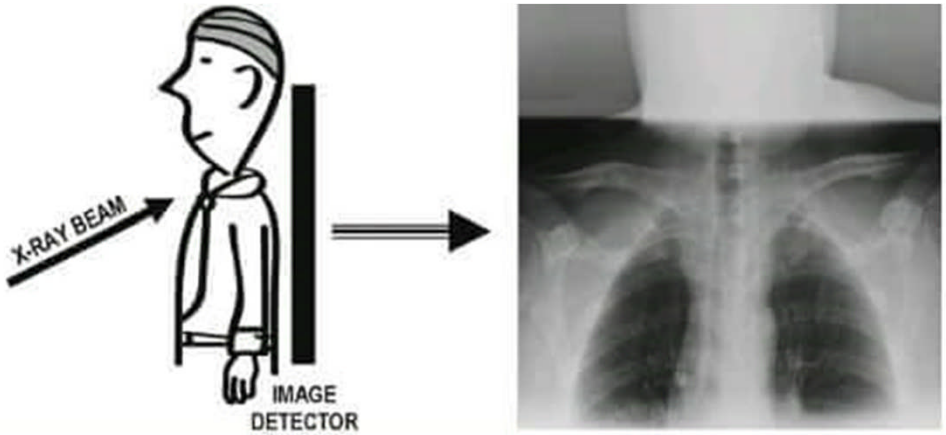

FIGURE 3.2 - THE LORDOTIC PROJECTION
The lordotic view is especially useful for visualizing the lung apices. The clavicles are projected cephalad, allowing a clear view of the lung apices

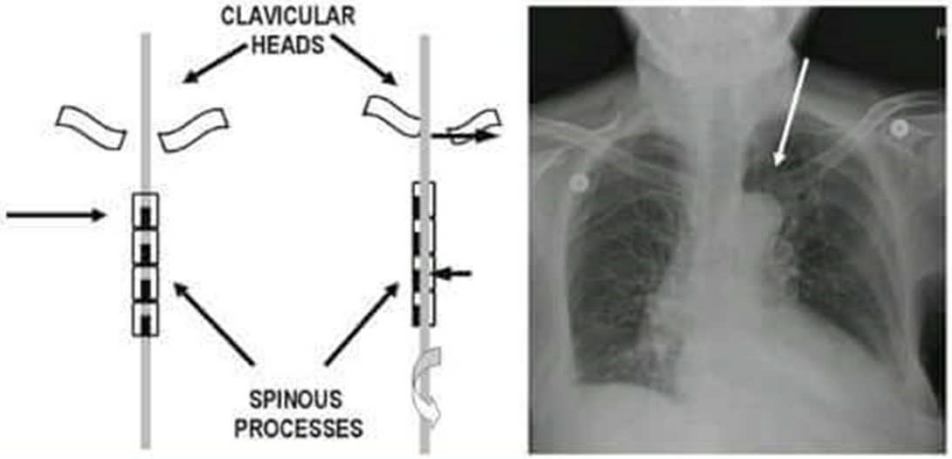

FIGURE 3.3 - ROTATION OF THE CHEST
In this illustration, note how the clavicle heads and spinous processes of the vertebral bodies appear in the AP position and with rotation of the chest to the left. On the chest X-ray, the *arrow* points to the left clavicular head, indicating that the patient is rotated to the left

FIGURE 3.5 - NORMAL KUB

FIGURE 3.6 - NORMAL BARIUM ENEMA

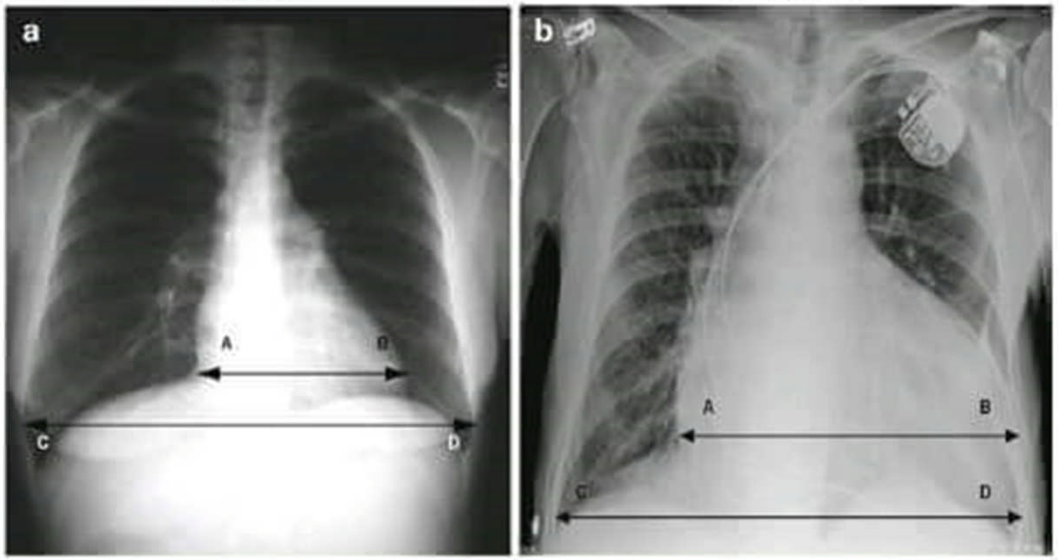

FIGURE 9.2 - MEASURING THE CARDIAC SILHOUETTE
(**a**) When evaluating the size of the heart, A–B should be 50–55% the measurement of C–D (the transverse thoracic diameter). (**b**) Shows marked enlargement of the cardiac silhouette with mild pulmonary vascular congestion. Note how the ratio of A–B to C–D is greater than 50%

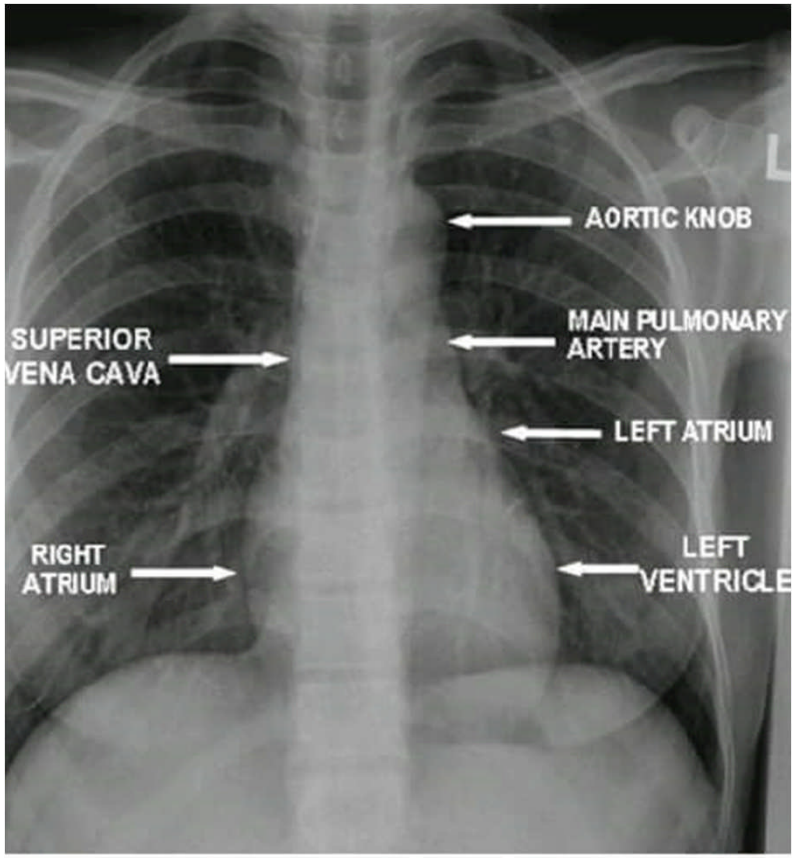

RE 9.1 - CARDIAC CONTOURS

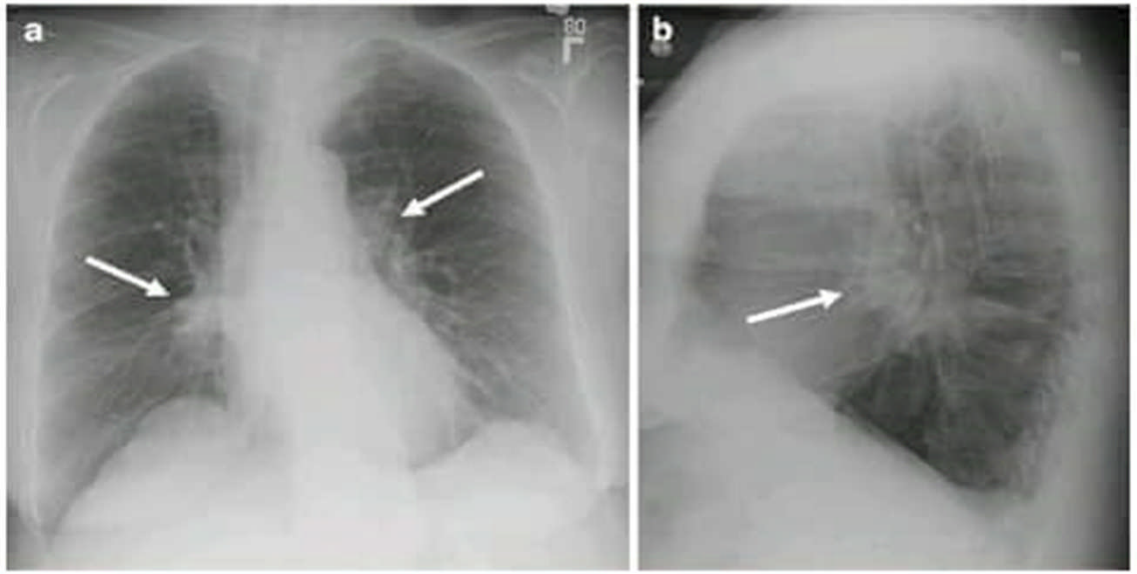

FIGURE 10.5 - HILAR ADENOPATHY
PA (**a**) and lateral (**b**) chest radiographs show a patient with hilar adenopathy (*arrows*)

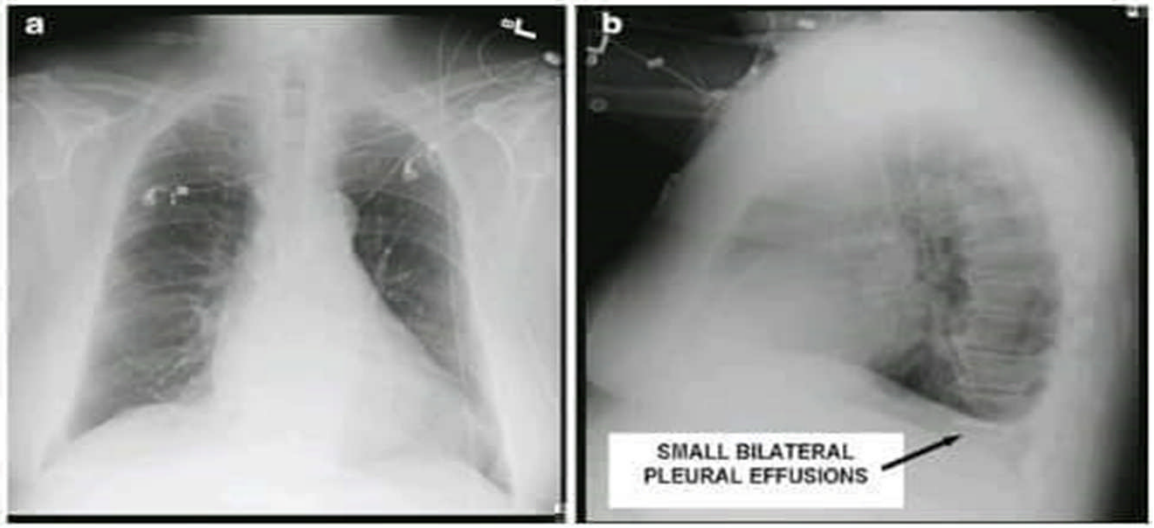

FIGURE 10.3 - BILATERAL PLEURAL EFFUSIONS FRONTAL (A) AND LATERAL (B) VIEWS OF A PATIENT WITH SUSPECTED BILATERAL PLEURAL EFFUSIONS
Note that although bilateral pleural effusions are clearly evident on the lateral projection, (b) the costophrenic angles are clear and sharp on the frontal view (a)

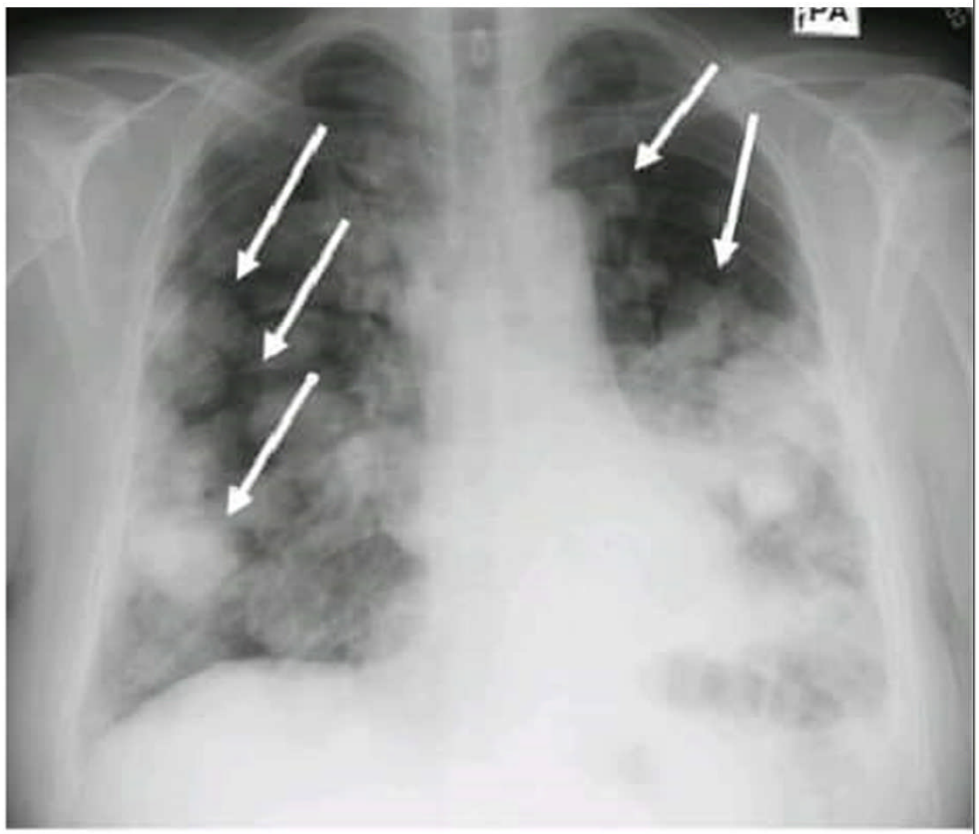

FIGURE 11.5 - PULMONARY NODULES
Frontal chest radiograph demonstrating numerous pulmonary nodules throughout both lung fields (*arrows*)

FIGURE 11.4 - CAVITARY LESION
Note the area of decreased density in the left upper lobe within the area of parenchymal disease

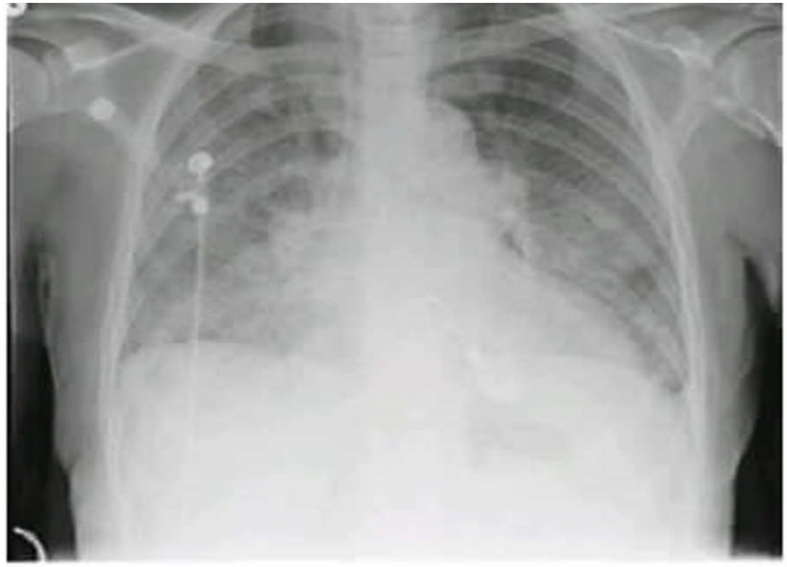

FIGURE 12.2 AIR SPACE CONSOLIDATION
Frontal chest radiograph demonstrating diffuse air space disease

Metastases

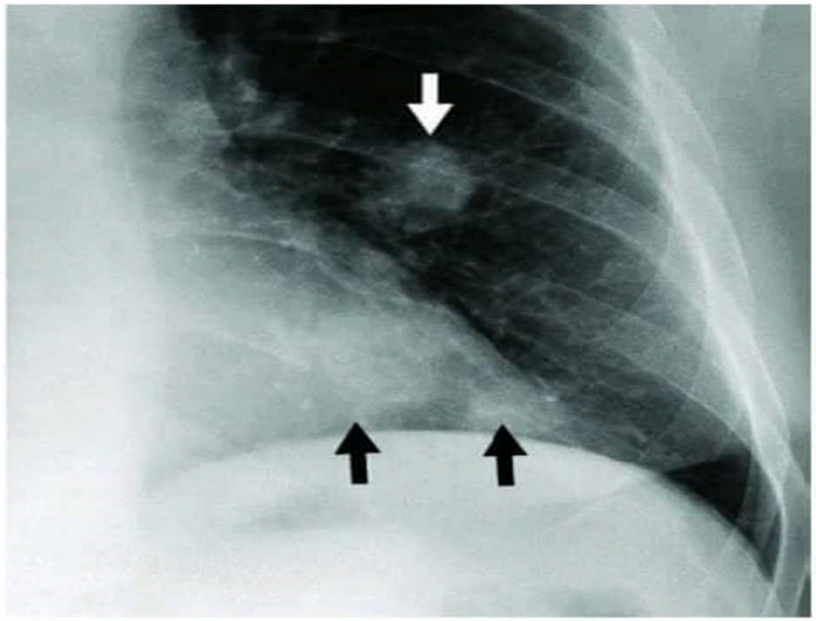

Fig. 6.17 This is what typical metastases (arrows) look like: multiple round nodules with relatively sharp margins surrounded by pulmonary parenchyma.

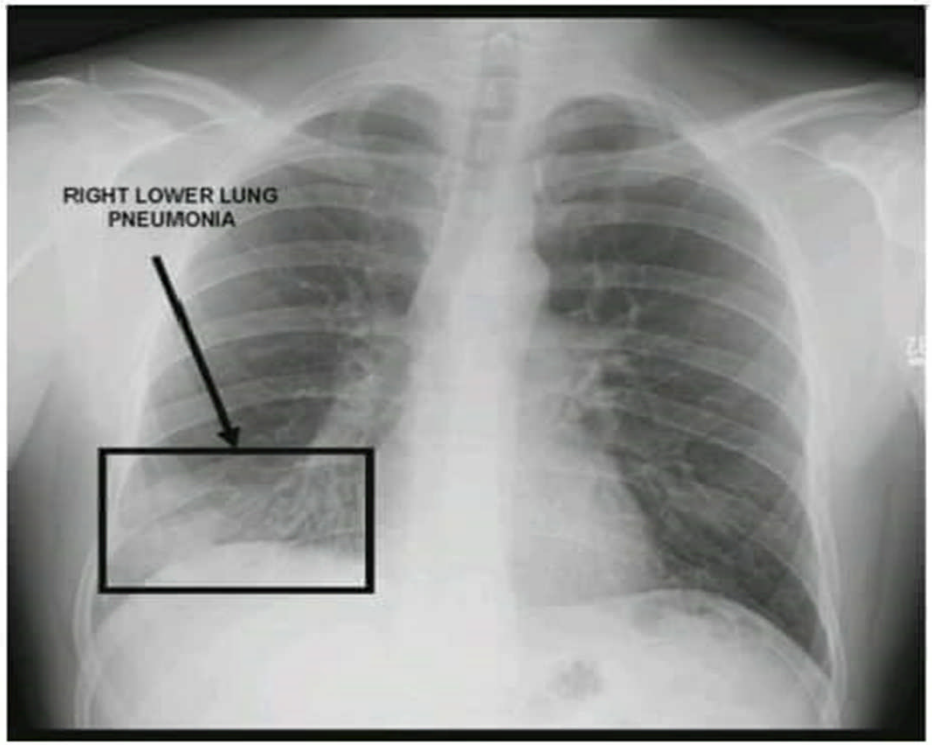

FIGURE 12.4 - PNEUMONIA Patchy airspace disease in the right lower lung consistent with pneumonia

Bronchial Carcinoma

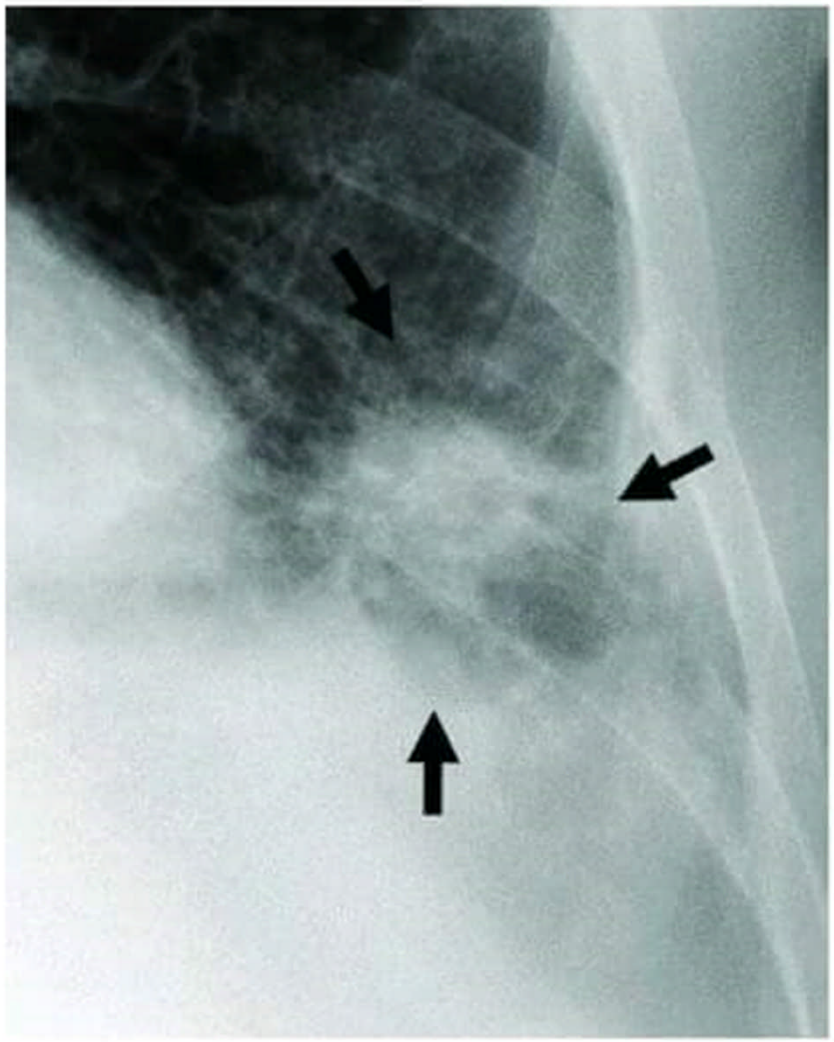

Fig. 6.**18** This bronchial carcinoma (arrows) has a spiculated border. The tumor invades and distorts the surrounding pulmonary parenchyma in the process (see also Fig. 6.**8a**).

Metastases of Testicular Carcinoma

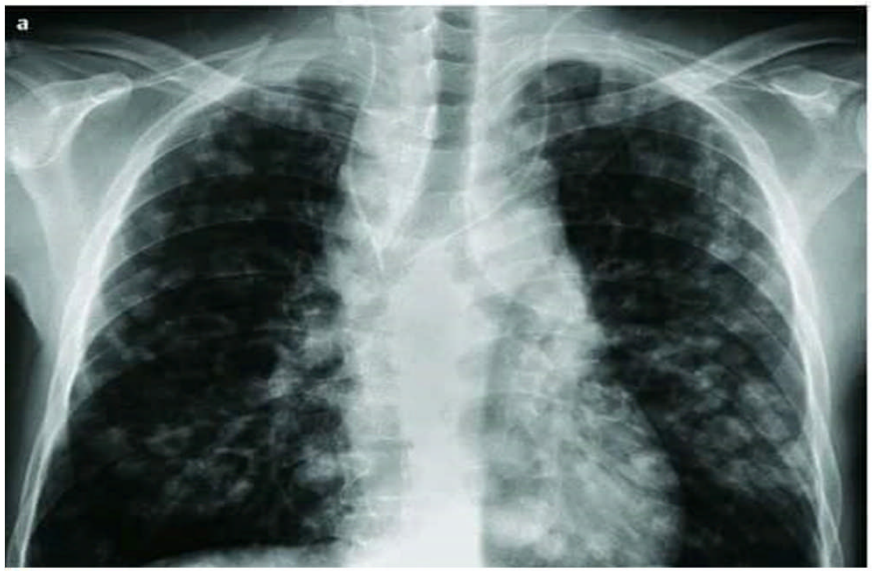

Hemothorax